Eur J Nucl Med Mol Imaging (2011) 38:1224–1236
DOI 10.1007/s00259-011-1760-x

ORIGINAL ARTICLE

^{68}Ga-DOTATOC PET/CT and somatostatin receptor (sst1–sst5) expression in normal human tissue: correlation of sst2 mRNA and SUV_{max}

Christian Boy · Till A. Heusner · Thorsten D. Poeppel · Anja Redmann-Bischofs · Nicole Unger · Walter Jentzen · Wolfgang Brandau · Klaus Mann · Gerald Antoch · Andreas Bockisch · Stephan Petersenn

Received: 16 July 2010 / Accepted: 3 February 2011 / Published online: 3 March 2011

Abstract
Purpose By targeting somatostatin receptors (sst) radiopeptides have been established for both diagnosis and therapy. For physiologically normal human tissues the study provides a normative database of maximum standardized uptake value (SUV_{max}) and sst mRNA.
Methods A total of 120 patients were subjected to diagnostic ^{68}Ga-DOTATOC positron emission tomography (PET)/CT (age range 19–83 years). SUV_{max} values were measured in physiologically normal tissues defined by normal morphology, absence of surgical intervention and absence of metastatic spread during clinical follow-up. Expression of sst subtypes (sst1–sst5) was measured independently in pooled adult normal human tissue by real-time reverse transcriptase polymerase chain reaction (RT-PCR).
Results SUV_{max} revealed a region-specific pattern (e.g., mean±SD, spleen 31.1±10.9, kidney 16.9±5.3, liver 12.8±3.6, stomach 7.0±3.1, head of pancreas 6.2±2.3, small bowel 4.8±1.8, thyroid 4.7±2.2, bone 3.9±1.3, large bowel 2.9±0.8, muscle 2.1±0.5, parotid gland 1.9±0.6, axillary lymph node 0.8±0.3 and lung 0.7±0.3). SUV_{max} was age independent. Gender differences were evident within the thyroid (female/male: 3.7±1.6/5.5±2.4, $p<0.001$; Mann-Whitney U test) and the pancreatic head (5.5±1.9/6.9±2.2, $p<0.001$). The sst mRNA was widely expressed and heterogeneous, showing sst1 to be most abundant. SUV_{max} values exclusively correlated with sst2 expression ($r=0.846$, $p<0.001$; Spearman rank correlation analysis), whereas there was no correlation of SUV_{max} with the expression of the other four subtypes.
Conclusion In normal human tissues ^{68}Ga-DOTATOC imaging has been related to the expression of sst2 at the level of mRNA. The novel normative database may improve diagnostics, monitoring and therapy of sst-expressing tumours or inflammation on a molecular basis.

Keywords Somatostatin receptors · sst · Somatostatin analogues · PET/CT · RT-PCR · Normal values

Electronic supplementary material The online version of this article (doi:10.1007/s00259-011-1760-x) contains supplementary material, which is available to authorized users.

C. Boy (✉) · T. D. Poeppel · W. Jentzen · W. Brandau · A. Bockisch
Department of Nuclear Medicine, University Hospital Essen, University of Duisburg-Essen,
Hufelandstraße 55,
45122 Essen, Germany
e-mail: christian.boy@uk-essen.de

T. A. Heusner · G. Antoch
Department of Diagnostic and Interventional Radiology and Neuroradiology,
University Hospital Essen, University of Duisburg-Essen,
45122 Essen, Germany

A. Redmann-Bischofs · N. Unger · K. Mann · S. Petersenn
Department of Endocrinology and Division of Laboratory Research, University of Duisburg-Essen,
45122 Essen, Germany

Introduction

Acting as first messengers, neuropeptides are required for cell-to-cell communication to modulate neurotransmission as well as somatic functions including tissue growth and apoptosis [1–4]. The neuropeptide somatostatin (SOM) is produced within the hypothalamus, throughout the central nervous system and in most peripheral organs by cells of the autonomous nervous, the neuroendocrine, the inflam-

matory and the immune systems [1, 2, 5]. Expression of somatostatin receptors (sst) and that of SOM are not always matched; SOM may act at the site of release, the post-synapse, adjacent cells, and via the circulation [1, 6, 35]. At the cellular level, sst have been found on the plasma membrane, but also in the cytosol, where they may either represent soluble forms of sst differing from the membrane species, receptor-mediated peptide internalization or simple turnover of receptors (receptor recycling) [2]. Five sst subtypes have been cloned and characterized to bind SOM with nanomolar affinity [1, 5–7]. All five receptor subtypes (sst1 to sst5) are G protein coupled sharing common signalling pathways [2, 3]. Moreover, subtype-specific effector mechanisms have indicated heterogeneity of sst functions [1, 3, 8]. Clinical and experimental studies have evidenced a pathogenetic involvement of SOM and sst in neoplasia; consequently, targeting tumours expressing sst subtypes with radiolabelled somatostatin agonists has become an established means for diagnosis, therapeutic monitoring and therapy [9–11]. Moreover, SOM and sst have also been shown to be involved in non-neoplastic pathological conditions, such as inflammation [12–15].

The somatostatin agonist ^{68}Ga-DOTATOC (^{68}Ga-1,4,7,10-tetraazacyclododecane-*N*,*N*′,*N*″,*N*‴-tetraacetic acid-D-Phe^{1}-Tyr^{3}-octreotide) and positron emission tomography (PET) (/CT) have been used successfully for diagnosis and therapeutic management of sst-expressing tumours [16–18]. In this respect, ^{68}Ga-DOTATOC uptake has been related to the expression of sst2 at the protein level as well as at the transcriptional level [19]. However, data on these relationships in physiologically normal tissue are few and partly lacking. Moreover, normal tissue uptake of ^{68}Ga-DOTATOC including age and gender differences has not been addressed in a large population. To date, several biodistribution studies using different somatostatin analogues have addressed regional tracer kinetics, however, mainly for dosimetry of tumour and normal tissues [14, 16, 20–22]. To establish a normative synoptic database, we applied two independent quantitative approaches to human sst, i.e. in vivo imaging with ^{68}Ga-DOTATOC PET/CT and measurement of sst expression by real-time reverse transcriptase polymerase chain reaction (RT-PCR).

Materials and methods

Patients

A total of 120 patients (female/male 60/60, age 53.8±12.7 years, range 19.1–83.0 years) who underwent routine diagnostic whole-body ^{68}Ga-DOTATOC PET/CT in our institution were enrolled in the retrospective analysis. General exclusion criteria were recent chemotherapy, therapy with somatostatin analogues or radiopeptides and systemic inflammatory or infectious diseases. In the selected 120 patients, the clinical indications for the PET/CT scan were confirmed or suspected sst-expressing malignancy, i.e. gastroenteropancreatic neuroendocrine tumour (NET) (n=66), other NET (n=28) and NET of unknown primary (n=26).

Radiopharmaceutical

Synthesis of ^{68}Ga-DOTATOC was performed according to the method previously described by Zhernosekov et al. [23]. ^{68}Ga was obtained from a ^{68}Ge/^{68}Ga radionuclide generator (Eckert & Ziegler, Berlin, Germany). Overall preparation time was about 60 min with a radiochemical yield of 60–70%. The mass of peptide (DOTATOC) applied per PET scan was 10±4 μg (range 3–20 μg). Quality control carried out with two thin-layer chromatography systems revealed a radiochemical purity of >98%. Routinely, sterility tests and bacterial endotoxin tests were performed after decay according to the European Pharmacopoeia out of the reference sample.

^{68}Ga-DOTATOC PET/CT

All patients had a full-dose, contrast-enhanced ("fully diagnostic") whole-body ^{68}Ga-DOTATOC PET/CT and did not receive positive oral contrast media but water-equivalent contrast. One hour before the examination, all patients received 1,000 ml of a water-equivalent oral contrast agent (0.2% locust bean gum and 2.5% mannitol dissolved in water). ^{68}DOTATOC PET/CT imaging was performed using a dedicated PET/CT system (Biograph Duo™, Siemens Medical Solutions, Hoffman Estates, IL, USA) composed of a dual-slice CT system (Somatom Emotion™, Siemens Medical Solutions, Forchheim, Germany) and a full-ring PET with bismuth germanate crystals (ECAT HR+™, Siemens Molecular Imaging, Hoffman Estates, IL, USA). CT was performed first, followed by PET. Whole-body CT (130 mAs, 130 kV, 5-mm sections, 8-mm table feed, 2.4-mm incremental reconstruction) covered a region ranging from just below the eyes to the upper thighs; 140 ml of an iodinated contrast material (Ultravist 300™, Schering AG, Berlin, Germany) was given intravenously at a flow rate of 3 ml/s for the first 90 ml and 1.5 ml/s for the remaining 50 ml (start delay 50 s). A limited breath-hold technique was used to avoid motion-induced artefacts. PET images were obtained after an uptake time of 66±36 min (range 24–308 min) after intravenous injection of 92±17 MBq (range 35–138 MBq) ^{68}Ga-DOTATOC.

Iterative algorithms [Fourier rebinning (FORE) and attenuation-weighted ordered subset expectation maximiza-

tion (AWOSEM), nonlinear] with 2 iterations and 8 subsets were used for image reconstruction, followed by a post-reconstruction 3-D Gaussian smoothing filter of 5-mm full-width at half-maximum (FWHM). Image reconstruction was performed with and without PET attenuation correction. Data obtained from CT were used for attenuation correction of the PET emission data. The default transverse emission images had 128×128 voxels with a transverse pixel size of 5.0×5.0 mm^2 and an axial slice width of 2.4 mm. The reconstructed spatial resolution for ^{68}Ga of the PET/CT system used was determined, a value needed to discuss aspects pertaining to partial volume effect. The detailed description of the resolution phantom, its measurement and reconstruction have been published by our group [24]. In short, a cylindrical phantom (20-cm axial length, 20-cm outside diameter) contained line sources orthogonal to the transverse plane (or parallel to the PET system axis). The cavity of the phantom was filled with non-radioactive water. The line source, consisting of a refillable polyethylene tubing (0.8-mm inner diameter), was looped back through the phantom to provide four distances of 1 and 7 cm from the central axis of the scanner's field of view (FOV): (x=1 cm, y=0), (x=7 cm, y=0), (x=0, y=1 cm), (x=0, y=7 cm). The transverse spatial resolution was determined at four positions each at the centre (z=0) and one fourth of the scanner's FOV (z=±1/4 FOV). The identical reconstruction algorithm and parameters were used as in the patient study, but the transverse emission images had 512×512 voxels with a voxel size of 0.53×0.53×2.0 mm^3. The image spatial resolution was expressed as FWHM. The width of the reconstructed line spread function in the tangential and radial directions was measured for each line source position. These line profiles were fitted with a Gaussian function. The average values in the tangential and radial directions obtained at transverse (1 and 7 cm) and axial positions (centre and ±1/4 FOV) were calculated.

Evaluation of target tissues in PET/CT

In each patient apparently normal target tissues were defined by normal morphology on the CT being part of the ^{68}Ga-DOTATOC PET/CT and normal history (including absence of surgery). Additionally, target tissues were excluded that were involved in metastatic spread during a clinical follow-up of 12 months. The following target tissues were defined for the determination of the maximum standardized uptake value (SUV_{max}): (r/l: right/left, paired organs): parotid gland (r/l), heart, lung (r/l), liver, spleen, stomach, small bowel (distal part of the duodenal "C"), large bowel (colon ascendens), pancreas (head, body, tail, uncinate process), thyroid gland, adrenal gland (r/l), kidney (whole organ volumes of interest; r/l), bone (T12 vertebra), muscle (erector spinae at T12), axillary (r/l) and inguinal (r/l) lymph nodes. First, the CT images were evaluated separately to exclude suspected tumours or non-neoplastic pathological conditions in target tissues. Attenuation-corrected PET images as well as PET/CT images were analysed. To exclude artificially elevated tracer uptake, the non-attenuation-corrected PET images were also read. For quantitative evaluation, SUV_{max} was measured using regions of interest drawn on the fused PET/CT (AW Suite™ Volume Viewer Plus™ software, GE Healthcare, Munich, Germany). Each target tissue or respective organ was entirely covered. In bilateral organs, such as adrenals, the mean SUV_{max} of right and left was calculated additionally. All PET/CT images were independently evaluated by three experienced physicians of the departments.

Tissue and RNA samples and quantitative real-time RT-PCR

Determination of sst (sst1–sst5) expression at the level of mRNA (RNA molecules/μg total RNA) was done as previously described by our group ([25–27]; see supplemental material). Total RNAs obtained from several human tissues were components of the Human Total RNA Master Panel II from BD Biosciences (BD Biosciences, Heidelberg, Germany). The adult tissues analysed were: brain, cerebellum, spinal cord, pituitary, thyroid gland*, adrenal gland*, heart*, trachea, lung*, pancreas*, liver*, spleen*, stomach*, small intestine*, colon*, kidney*, testis, prostate, ovary, uterus, placenta, salivary gland*, skeletal muscle* and bone marrow* (*tissue sample anatomically matching a respective target region of the PET/CT).

Statistical analysis and data evaluation

Data are expressed as mean±SD. All statistical analyses were performed using commercial software (IBM SPSS Statistics 18, SPSS Inc., Chicago, IL, USA). Following one-way analysis of covariance (ANCOVA) of SUV_{max} data with laterality (in bilateral organs), age, gender, mass (of DOTATOC) and uptake time (interval between tracer injection and PET acquisition) as covariates, differences between the means of two variables were evaluated by the two-sided Mann-Whitney U test. Associations of somatostatin receptor expression between sst subtypes and with regional SUV_{max} (uptake data of 120 subjects) were tested by two-sided Spearman rank correlation analysis. A value of $p<0.05$ was considered statistically significant. To account for multiple comparisons, the Bonferroni method was applied.

Results

^{68}Ga-DOTATOC imaging

Regional tracer accumulation was heterogeneous within the 120 subjects studied (Fig. 1) with the highest uptake of ^{68}Ga-DOTATOC within the spleen. Scatter plots of regional SUV_{max} data were displayed in logarithmic scale (Fig. 2). There were no significant influences of the covariates age, tracer mass, uptake time and laterality on SUV_{max}. Consequently, in bilateral organs averaged data of right and left sides were used for further analyses. However, 2 of the 19 target regions studied by PET/CT revealed significant gender differences: in the thyroid gland, SUV_{max} of male subjects exceeded that of female subjects by about 50% (female/male 3.7±1.6/5.5±2.4, $p<0.001$, Mann-Whitney U test) and in the pancreatic head by about 25%, respectively (female/male 5.5±1.9/6.9±2.2, $p<0.001$). Descriptive statistics of regional SUV_{max} data are diplayed in Tables 1, 2 and 3. Within the entire population of 120 subjects (Table 1) three major categories of tracer uptake were evident: regions with a physiologically low mean uptake ($SUV_{max}<1$; e.g. lymph nodes and lung), high uptake regions (SUV_{max} >10; e.g. liver, adrenals, kidneys and spleen) and "intermediate" regions with SUV_{max} values ranging between the latter two groups. SUV_{max} values covered a wide range, with spleen demonstrating the highest value approximately two orders of magnitude higher than lung tissue. However, for each tissue, SUV_{max} values demonstrated a remarkably low variability with coefficients of variation between 25 and 48%. Regions with intermediate uptake revealed slight and, partly, significant differences (Tables 1 and 3). For instance, in the gut SUV_{max} decreased towards the colon. Moreover, the pancreas head and, especially, the uncinate process tended towards higher SUV_{max} values than pancreatic body or tail. Notably, with the exception of the suprarenal gland, SUV_{max} of the liver significantly differed from that of all other regions. Additionally, considering the intended clinical use of the present normative database, SUV_{max} data were evaluated for those subjects measured within a strict time window of 30–90 min post-injection (Table 2; n=99, female/male 48/51; age 55.5± 12.9 years, range 19.1–83.0 years, time post-injection 55.5± 14.7 min, range 31–90 min); likewise, for this subgroup ANCOVA did not reveal influences of age, tracer mass, uptake time and laterality on SUV_{max}. As displayed in Table 2, regional SUV_{max} values were comparable to that of the whole population with slightly different variation coefficients (e.g. in the subgroup the uncinate process SUV_{max} was significantly different from that of all other pancreatic tissues including pancreas tail region). Moreover, in this subgroup, gender differences appeared to be limited to the thyroid (female/male 3.7±1.6/5.4±2.6, range 1.1–7.6/2.6–14.3; $p<0.001$, Mann-Whitney U test).

Transverse spatial resolution

The transverse spatial resolution for ^{68}Ga was 8.1±0.3 mm. For comparison, the published transverse spatial resolution for the mean±standard deviation FWHM values for [^{18}]F was 7.4±0.2 mm [24]. A small degree of resolution degradation of ~1 mm was observed for ^{68}Ga versus [^{18}]F caused by the larger positron energy.

Normal tissue SUV_{max} and sst expression

Table 4 depicts a quantitative synopsis of regional sst transcription. The most abundant somatostatin receptor subtype in the human body was sst1 with an average 1.3×10^5 copies/μg RNA in the tissues analysed, demonstrating significantly higher expression than sst3 (108×), sst4 (30×) and sst5 (3×); sst2 was nearly as abundant as sst1 with 1.1×10^5 copies/μg RNA, significantly higher than sst3

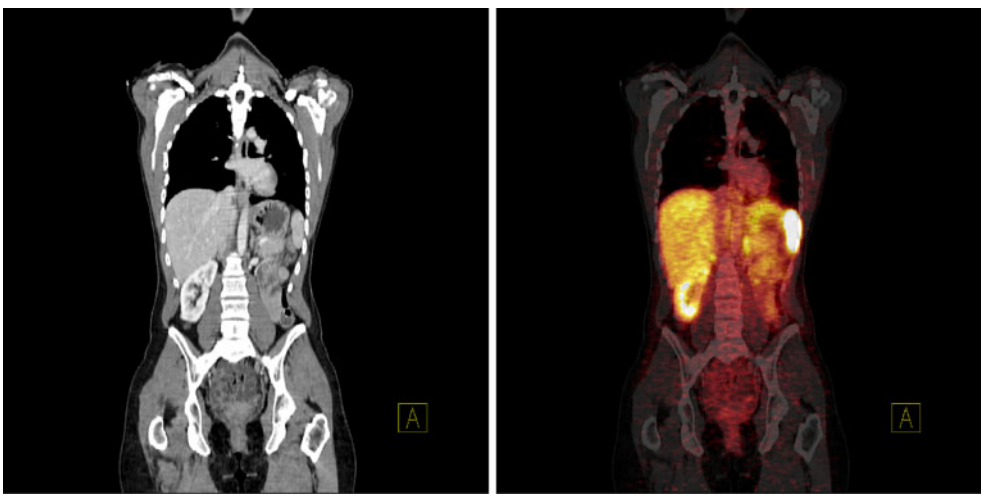

Fig. 1 Representative ^{68}Ga-DOTATOC whole-body scan. Contrast-enhanced CT (*left*) and PET/CT fusion (*right*)

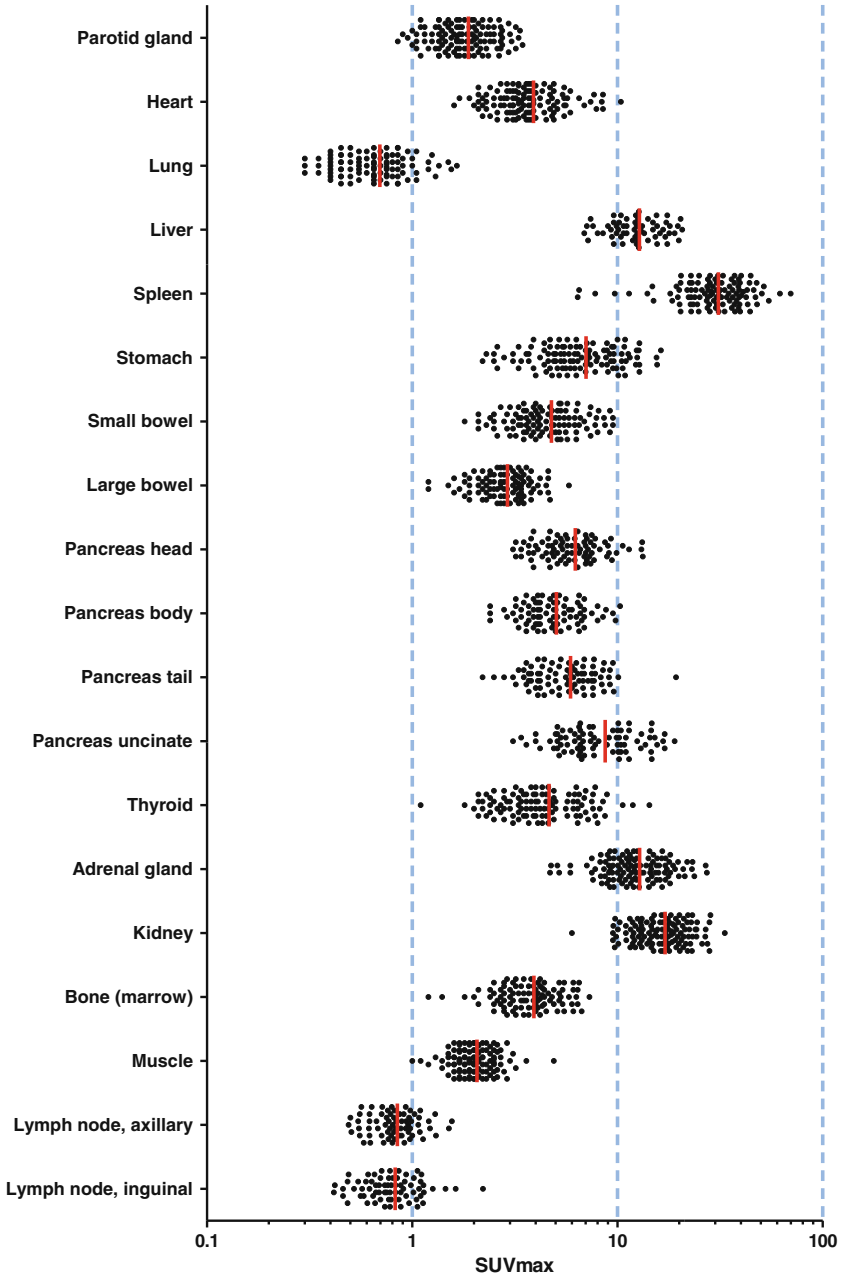

Fig. 2 For the whole population of subjects ($n=120$) SUV_{max} of ^{68}Ga-DOTATOC (log scale) scatter-plotted by region. The *red bar* identifies the group mean

and sst4 as the least abundant receptor subtypes (1.3×10^3 and 4.4×10^3 copies/μg RNA, respectively). The sst5 copies ranged in between with 5.2×10^4 copies/μg RNA on average. We found marked region-dependent heterogeneities of both global sst expression and relative fractions of sst subtypes. When comparing the various tissues, somatostatin receptor expression was most abundant within the central nervous system (brain and cerebellum), pituitary, the adrenals and the stomach (all $>1\times10^5$ copies/μg RNA on average), compared to the least abundant in heart, testis, placenta, trachea, thyroid, lung, muscle, salivary gland and bone marrow (all $<1\times10^4$ copies/μg RNA on average). Expression levels in small intestine, kidney, spinal cord, ovary, liver, colon, uterus, spleen, prostate and pancreas ranged in between. When comparing the relative subtype distribution in various tissues, descriptive statistics revealed strong predominance of sst1 in stomach, small intestine, liver, colon, placenta and lung (all with sst1>90% of all five ssts, compared to an average of 56%). For sst2, predominant expression in relation to the other subtypes was found in cerebellum, spleen, salivary gland and bone marrow (all with sst2>60%, compared to an average of 29%); sst3 and sst4 were relatively predominant in testis (>10%, compared to an average of 1% for both subtypes) and sst5 in pituitary, adrenals, ovary and pancreas (>40%, compared to an average of 13%).

Table 1 Regional ^{68}Ga-DOTA-TOC SUV_{max} values displayed for the whole population (n=120)

Regional SUV_{max}, entire population	n	Mean	SD	Min.	Max.	Mean − 2 SD	Mean+2 SD
Parotid gland	118	1.9	0.6	0.9	3.5	0.7	3.1
Heart	118	3.9	1.6	1.6	10.4	0.8	7.0
Lung	98	0.7	0.3	0.3	1.7	0.1	1.3
Liver	62	12.8	3.6	6.9	20.7	5.6	20.0
Spleen	108	31.1	10.9	6.4	69.8	9.2	52.9
Stomach	113	7.0	3.1	2.2	16.3	0.8	13.3
Small bowel	105	4.8	1.8	1.8	9.5	1.1	8.4
Large bowel	98	2.9	0.8	1.2	5.8	1.2	4.6
Pancreas head	82	6.2	2.3	3.1	13.3	1.7	10.8
Pancreas body	81	5.1	1.7	2.4	10.3	1.6	8.5
Pancreas tail	82	5.9	2.4	2.2	19.3	1.1	10.7
Pancreas uncinate	82	8.7	3.7	3.1	19.0	1.2	16.2
Thyroid	108	4.7	2.2	1.1	14.3	0.2	9.1
Adrenal gland	117	12.8	4.6	4.7	27.3	3.7	21.9
Kidney	119	16.9	5.3	6.0	33.4	6.4	27.5
Bone (marrow)	98	3.9	1.3	1.2	7.3	1.4	6.5
Muscle	117	2.1	0.5	1.0	4.9	1.0	3.1
Lymph node, axillary	72	0.8	0.3	0.5	1.6	0.3	1.4
Lymph node, inguinal	72	0.8	0.3	0.4	2.2	0.2	1.5

Figure 3 displays mRNA expression within the 14 respective tissues with matched target tissues in PET/CT. In analogy to the clinical PET routine procedure to compare an area of interest with liver uptake, both PET and PCR data were normalized. The expression of sst subtypes (sst1–sst5) was normalized to that of sst2 measured in liver tissue (Figs. 3 and 4). Similarly, SUV_{max} data were normalized to liver (Fig. 4 and Table 5). In direct comparison of PET/CT and RT-PCR data the SUV_{max} values correlated significantly and exclusively with sst2 expression, whereas there was no correlation with the expression of the other four subtypes.

Table 2 Regional ^{68}Ga-DOTA-TOC SUV_{max} values displayed for subjects measured 30–90 min post-injection (n=99)

Regional SUV_{max}, subgroup analysis 30–90 min post-injection	n	Mean	SD	Min.	Max.	Mean − 2 SD	Mean+2 SD
Parotid gland	97	1.9	0.6	0.9	3.5	0.7	3.1
Heart	97	3.9	1.7	1.6	10.4	0.6	7.3
Lung	80	0.7	0.3	0.3	1.7	0.1	1.3
Liver	51	13.0	3.8	6.9	20.7	5.3	20.7
Spleen	90	30.4	11.2	6.4	69.8	8.1	52.8
Stomach	95	7.0	3.1	2.2	15.6	0.7	13.3
Small bowel	85	4.8	1.9	2.1	9.5	1.1	8.5
Large bowel	83	3.0	0.8	1.2	5.8	1.3	4.7
Pancreas head	68	6.3	2.3	3.1	13.2	1.8	10.8
Pancreas body	68	5.2	1.8	2.4	10.3	1.7	8.7
Pancreas tail	68	6.1	2.4	2.5	19.3	1.2	11.0
Pancreas uncinate	68	8.7	3.7	3.4	19.0	1.2	16.2
Thyroid	87	4.6	2.4	1.1	14.3	-	9.3
Adrenal gland	96	12.9	4.8	4.7	27.3	3.3	22.4
Kidney	97	16.9	5.2	6.0	33.4	6.4	27.4
Bone (marrow)	81	3.9	1.3	1.2	7.3	1.3	6.4
Muscle	96	2.1	0.5	1.0	4.9	1.0	3.1
Lymph node, axillary	56	0.9	0.2	0.5	1.6	0.4	1.3
Lymph node, inguinal	56	0.8	0.3	0.4	2.2	0.3	1.4

Table 3 Differences between the means of regional ^{68}Ga-DOTATOC SUV_{max} values (Tables 1 and 2) evaluated by the two-sided Mann-Whitney U test

Region	Parotid gland	Heart	Lung	Liver	Spleen	Stomach	Small bowel	Large bowel	Pancreas head	Pancreas body	Pancreas tail	Pancreas uncinate	Thyroid	Adrenal gland	Kidney	Bone (marrow)	Muscle	Lymph node, axillary	Lymph node, inguinal
Parotid gland	-																		
Heart	a, b	-																	
Lung	a, b	a, b	-																
Liver	a, b	a, b	a, b	-															
Spleen	a, b	a, b	a, b	a, b	-														
Stomach	a, b	a, b	a, b	a, b	a, b	-													
Small bowel	a, b	a, b	a, b	a, b	a, b	a, b	-												
Large bowel	a, b	a, b	a, b	a, b	a, b	a, b	a, b	-											
Pancreas head	a, b	a, b	a, b	a, b	a, b		a, b	a, b	-										
Pancreas body	a, b	a, b	a, b	a, b	a, b	a, b	a	a, b	a, b	-									
Pancreas tail	a, b	a, b	a, b	a, b	a, b	a	b	a, b	a, b	a	-								
Pancreas uncinate	a, b	a, b	a, b	a, b	a, b	b	a, b	a, b	b	a, b	b	-							
Thyroid	a, b		a, b	a, b	a, b	a, b		a, b	a, b	a	b	a, b	-						
Adrenal gland	a, b	a, b	a, b		a, b	a, b	a, b	a, b	a, b	a, b	a, b	a, b	a, b	-					
Kidney	a, b	a, b	a, b	a, b	a, b	a, b	a, b	a, b	a, b	a, b	a, b	a, b	a, b	a, b	-				
Bone (marrow)	a, b		a, b	a, b	a, b	a, b	a, b	a, b	a, b	a, b	a, b	a, b		a, b	a, b	-			
Muscle	a	a, b	a, b	a, b	a, b	a, b	a, b	a, b	a, b	a, b	a, b	a, b	a, b	a, b	a, b	a, b	-		
Lymph node, axillary	a, b	a, b	a, b	a, b	a, b	a, b	a, b	a, b	a, b	a, b	a, b	a, b	a, b	a, b	a, b	a, b	a, b	-	
Lymph node, inguinal	a, b	a, b	a, b	a, b	a, b	a, b	a, b	a, b	a, b	a, b	a, b	a, b	a, b	a, b	a, b	a, b	a, b		-

Mann-Whitney U test: [a] Bonferroni-adjusted $p<0.05$ (entire study population, $n=120$, data displayed in Table 1); [b] Bonferroni-adjusted $p<0.05$ (subjects measured after 30–90 min post-injection, $n=99$, data displayed in Table 2)

Table 4 Real-time RT-PCR data reflecting regional somatostatin expression of sst subtypes (sst1–sst5) (mRNA copy numbers per microgram of total RNA). Additionally, fractional composition of each region by somatostatin receptor subtypes (%) is shown. Asterisks indicate tissue samples that match a corresponding target tissue in ^{68}Ga-DOTATOC PET/CT

Tissue sample	sst1	sst2	sst3	sst4	sst5	sst1 (%)	sst2 (%)	sst3 (%)	sst4 (%)	sst5 (%)
Brain	723,261	417,658	1,880	27,795	1,985	61.7	35.6	0.2	2.4	0.2
Cerebellum	50,144	1,158,699	2,366	66,861	233,789	3.3	76.6	0.2	4.4	15.5
Spinal cord	188,169	120,432	1,407	1,150	19,258	56.9	36.4	0.4	0.3	5.8
Pituitary	135,043	310,500	459	439	349,151	17.0	39.0	0.1	0.1	43.9
Thyroid*	14,104	11,541	25	270	196	54.0	44.2	0.1	1.0	0.7
Adrenal*	74,289	233,495	15,730	153	384,154	10.5	33.0	2.2	0.0	54.3
Heart*	33,781	5,019	25	563	6,732	73.2	10.9	0.1	1.2	14.6
Trachea	19,877	7,066	25	117	10,026	53.6	19.0	0.1	0.3	27.0
Lung*	20,387	258	25	674	25	95.4	1.2	0.1	3.2	0.1
Pancreas*	45,354	4,784	267	25	44,330	47.9	5.0	0.3	0.0	46.8
Liver*	199,494	12,131	25	25	132	94.2	5.7	0.0	0.0	0.1
Spleen*	19,312	78,590	70	563	25	19.6	79.7	0.1	0.6	0.0
Stomach*	576,631	41,895	147	417	10,598	91.6	6.7	0.0	0.1	1.7
Small intestine*	434,094	23,786	30	527	1,046	94.5	5.2	0.0	0.1	0.2
Colon*	167,608	6,742	46	1,137	288	95.3	3.8	0.0	0.6	0.2
Kidney*	213,534	139,757	25	33	5,910	59.4	38.9	0.0	0.0	1.6
Testis	11,119	19,438	5,382	4,510	4,695	24.6	43.1	11.9	10.0	10.4
Prostate	54,561	37,234	25	155	3,603	57.1	39.0	0.0	0.2	3.8
Ovary	41,421	4,743	1,226	25	177,175	18.4	2.1	0.5	0.0	78.9
Uterus	103,519	13,029	103	788	188	88.0	11.1	0.1	0.7	0.2
Placenta	37,058	3,499	25	425	134	90.1	8.5	0.1	1.0	0.3
Salivary gland*	2,025	4,638	25	25	592	27.7	63.5	0.3	0.3	8.1
Skeletal muscle*	8,323	949	25	40	25	88.9	10.1	0.3	0.4	0.3
Bone (marrow)*	1,408	3,544	25	54	25	27.9	70.1	0.5	1.1	0.5

Discussion

To our knowledge, the present study is the first approach to generate a dedicated normal tissue database of human sst expression at both the receptor site by means of in vivo ^{68}Ga-DOTATOC PET/CT and the mRNA level by ex vivo RT-PCR, each applied for large subject populations.

Methodological considerations and parameters chosen

PET/CT, SUV_{max} and recovery correction The noninvasive PET/CT approach by measurement of regional SUV_{max} is a common part of (semi-)quantitative diagnostic procedures [28]. Using SUV_{max} is a simple approach to determine the uptake properties of tissues with a single PET measurement,

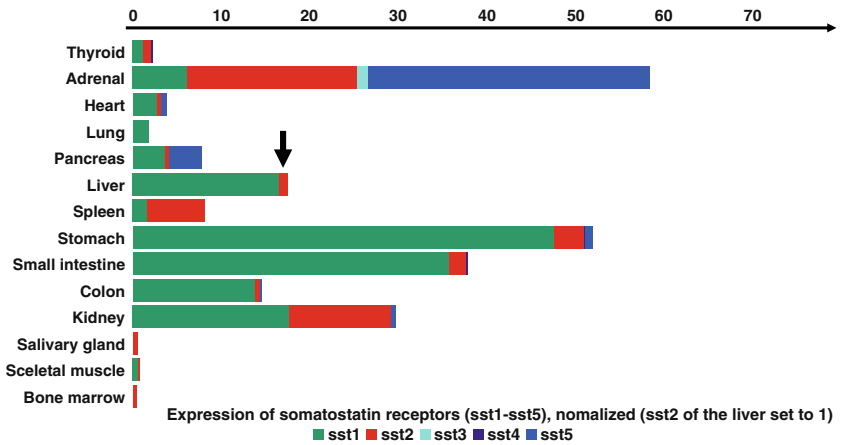

Fig. 3 Normalized regional expression of somatostatin receptor subtypes (sst1–sst5) at the mRNA level. The dimensionless x-axis displays quantitative RT-PCR data of regional somatostatin receptor expression (mRNA copy numbers per microgram of total RNA) divided by the expression of sst2 in the liver. Thus, the liver has a normalized sst2 expression of one (*arrow*). Only tissue samples are displayed (n=14) that have a corresponding target region in PET/CT

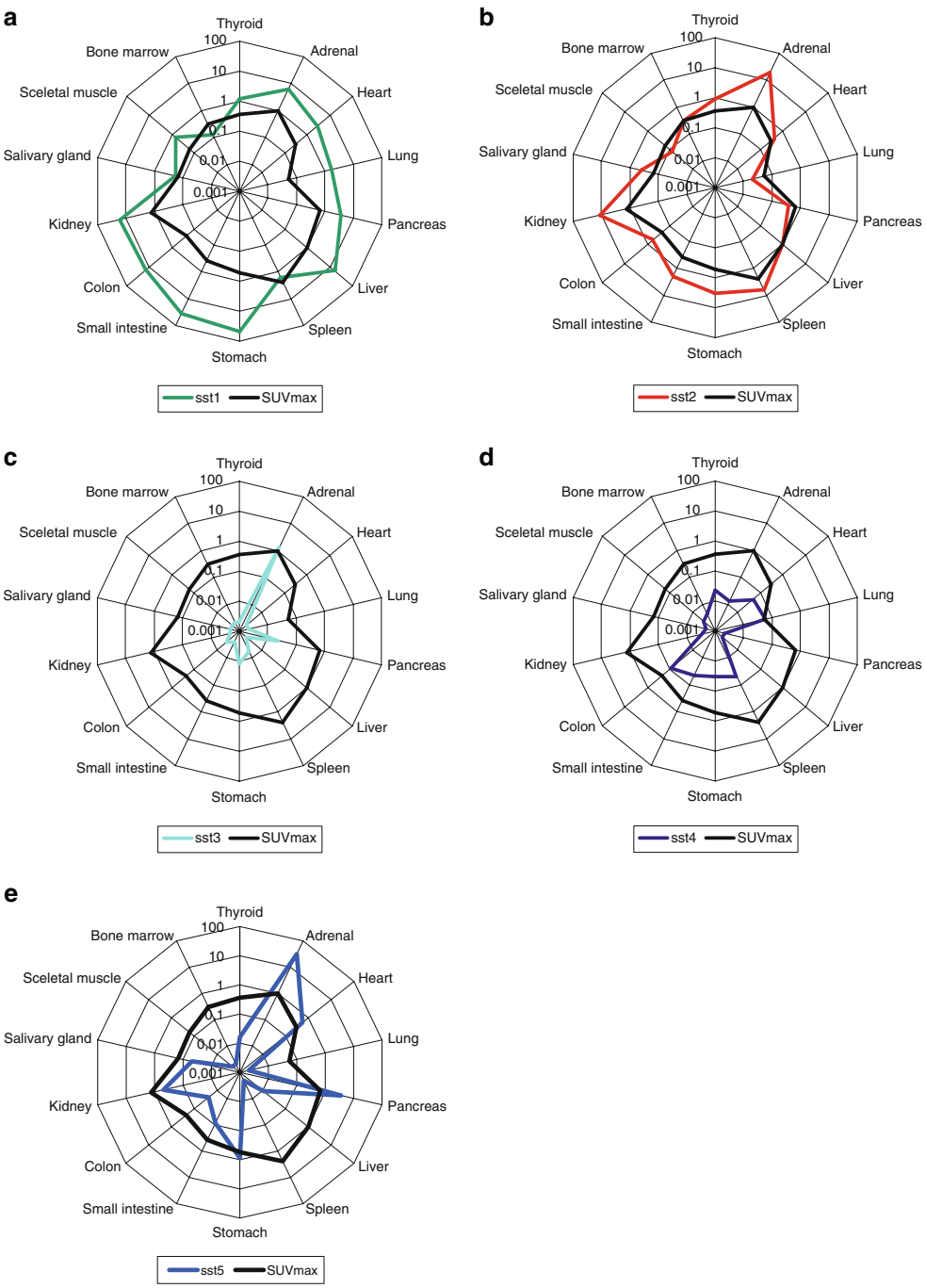

Fig. 4 a–e Polar plots (log scale) display the relation of regional ^{68}Ga-DOTATOC SUV_{max} values and the expression of somatostatin receptor subtypes (sst1–sst5). In each plot the *coloured line* displays the regional normalized subtype-specific receptor expression, i.e. regional mRNA copy numbers divided by sst2 mRNA copy numbers in the liver. The *black line* reflects the mean regional SUV_{max} divided by that of the liver. Thus, sst2 expression of liver and SUV_{max} of liver have been set to a value of one. SUV_{max} correlated significantly with sst2 expression (**b**), whereas there was no correlation with the expression of the other four subtypes (**a**, **c**–**e**). Spearman rho correlation coefficients and *p* values are shown in Table 5

whereas dynamic PET measurements and arterial blood sampling revealed detailed uptake kinetics [29], but may be unsuitable in routine clinical practice. Principally, the direct molecular target of ^{68}Ga-DOTATOC is the sst receptor protein. It has to be noted that the parameter chosen in the present study, i.e. SUV_{max}, does not singularly represent receptor-mediated processes. Depending on the organ studied, non-somatostatin receptor-mediated uptake may also contribute to the measured SUV values, especially in organs related to metabolism and elimination of the radiotracer like liver or kidney [30].

There are some general drawbacks using a maximum value such as SUV_{max} as described by our group [24]. First, since all the SUV data presented in this study are obtained from images, the SUV_{max} may be affected by the partial volume effect, in particular for small objects. In general, the level of the recovery correction depends on the ratio of object size to the scanner's spatial resolution. Knowing the spatial resolution is essential to estimate the partial volume correction. In this study, the reconstructed spatial resolution of ^{68}Ga in water was 8.1 mm. The fundamental work by Kessler et al. [31] showed that the imaged maximum voxel

Table 5 Relation of regional expression of somatostatin receptor subtypes (sst1–sst5) of 14 tissue samples versus ^{68}Ga-DOTATOC SUV_{max}: Spearman rho correlation coefficients (p, two-sided)

	vs sst1	vs sst2	vs sst3	vs sst4	vs SUV_{max}
sst1					0.464 (0.095)
sst2	0.635 (0.015)				0.846 (0.0001)*
sst3	0.436 (0.119)	0.509 (0.063)			0.489 (0.076)
sst4	0.097 (0.742)	0.033 (0.911)	0.155 (0.597)		−0.238 (0.413)
sst5	0.564 (0.035)	0.491 (0.075)	0.560 (0.037)	−0.194 (0.500)	0.340 (0.234)

*Correlation significant, Bonferroni-adjusted $p<0.05$

value is identical with the true maximum voxel value if the object diameter is larger than about three times the scanner resolution. As a consequence, the authors assume for the organs numbered with 1 to 17 (see Tables 1 and 2) no partial volume effect. In contrast, a significant partial volume effect was expected for normal lymph nodes. For example, an imaged SUV_{max} of 0.8 for a typically sized lymph node with a diameter of about 4 mm and a spatial resolution of about 8 mm would have a recovery-corrected SUV_{max} of about 17 [24]. Second, when an iterative reconstruction algorithm at low activity concentration regimes (about 1 kBq/ml) is used, the imaged SUV_{max} is overestimated by about 40% [24]. This low count statistics effect can also be expected for the SUV_{max} of the lymph nodes. Overall, taking into account both effects, the "true" SUV_{max} would be then effectively about 10. Thus, this methodological consideration shows that the true SUV_{max} of normal sized lymph node is about one order of magnitude higher than the image-derived SUV_{max}.

In vivo study design The use of "apparently normal" target tissues of patients for the SUV_{max} measurement is a compromise, since a pathological validation of healthy organs was not practicable. Moreover, the influence of putatively important cofactors, e.g. inflammation, carcinoid heart disease or cachexia, could only lead to the exclusion of a certain target tissue when reflected by diagnostic evidence (anamnestic data, examination, patient file, laboratory data and diagnostic CT) or pathology at the time of the PET/CT or during follow-up of 1 year. Thus, the retrospective design of the study may lead to limitations and the authors are aware that especially inflammatory changes in different target tissues may be minimized but not entirely excluded. Finally, the use of healthy volunteers instead of patients for PET/CT would not be suitable taking into account subject numbers and age ranges needed as well as issues of radiation protection. For the present study protocol, a significant bias of normal tissue SUV_{max} values by the mass of peptide applied, uptake time post-injection or by averaging bilateral organs could be excluded. Considering the variation in the time of the acquisition post-injection we included an analysis of all subjects studied within 30–90 min post-injection, i.e. a time window used in routine clinical practice.

In vitro studies To study sst expression in human tissue samples different molecular means have been established, i.e. measurement of sst expression at the mRNA level by RT-PCR [26] or at the level of the receptor protein using receptor immunohistochemistry [32]. In this context, immunohistochemistry may reveal high spatial resolution and specific binding of the phenotype, however, with very limited options to quantify. On the other hand, real-time RT-PCR may provide quantitative data of transcription at the price of morphology. Consequently, organ-specific distribution of sst may not be studied in detail using RT-PCR, e.g. within medulla and cortex of kidney or adrenal gland. Previous studies of our group using sst RT-PCR in normal tissue, tumour tissue and tumour cell lines have already addressed the clinical impact of sst mRNA data for receptor-targeted chemotherapeutic peptide antagonists and receptor immunohistochemistry and their potential future use in antineoplastic therapy [25]. In the present study RT-PCR assays were done in whole-body coverage, in contrast to the radiotracer ^{68}Ga-DOTATOC that cannot pass an intact blood-brain barrier. Due to methodological reasons the impact of the putative covariates age and gender could not be tested for the RT-PCT data. Moreover, despite a considerable number of clinical studies addressing regional expression of sst subtypes at the protein level or at the mRNA level (e.g. central nervous system, adrenals and gastrointestinal tract), normal tissue data have been limited and conflicting data must be considered, e.g. due to methodological differences, or low numbers of subjects or organs studied. For that reason, our study intended to gain RT-PCR or PET/CT data for a large number of normal tissues in a single methodological approach.

Comparison of in vivo and in vitro results Finally, the visualization and comparison of neurochemical profiles using polar plots of "receptor fingerprints" is an established

procedure to map receptors within the central nervous system [33]. Due to the clinical intention of the normative database, liver-based normalization of SUV_{max} and mRNA data was performed as an analogy to the practical routine of using the liver as a reference in the visual assessment of sst scintigraphies.

Normal tissue SUV_{max} and sst expression

In our study two different parameters and dimensions (SUV_{max} and mRNA copy numbers) have provided regional biochemical "fingerprints" of normal human tissue which have to be reflected in the context of known chemoarchitecture of SOM and sst. Regional distribution of somatostatinergic cells and sst and its functional implications under normal and pathological conditions are still within the focus of intensive clinical and experimental research. After detection of somatostatinergic processes in all vertebrates as well as in some invertebrate species, animal models have revealed significant species differences of regional sst expression and function [3, 34, 35]. Clinical and experimental data have evidenced a regional complex physiology of multiple partly coexpressed sst subtypes and interacting effector mechanisms. Human sst have appeared to be widely expressed with distinct but overlapping expression patterns [3]. Within the human body SOM-producing cells occur at high densities throughout the central and peripheral nervous systems, in the endocrine pancreas, and in the gut and in small numbers in the thyroid, adrenals, salivary glands, kidneys, prostate and placenta [6, 32, 35, 36]. Morphologically, gastrointestinal SOM-producing cells (D cells) have been located with the highest densities (>30 cells/mm^2) within the pancreas and lower densities within the mucosa of stomach, duodenum and ileum showing a general decrease in the anal direction. The gradual decrease of D cell density is paralleled by declining tissue concentrations of SOM as shown in bioptic material [37]. Besides D cell-related production, SOM is found in the autonomous nervous system, especially within the submucous and myenteric plexus [6]. In line with previous data on human sst expression, both SUV_{max} and sst expression partly followed the chemoarchitecture of SOM-producing cells in humans [1, 5–7, 35, 38]. As presented, both RT-PCR and SUV_{max} data were in good agreement with organ-specific reports on sst expression, e.g. of heart [38] and kidney [35] and the known biodistribution of ^{68}Ga-DOTATOC [16].

Diagnostic and therapeutic implications

Considering the diagnostic and therapeutic implications, a normative database should further characterize the profile of ^{68}Ga-DOTATOC with considerable affinities to three of five sst subtypes (sst2, sst3 and sst5) [9]. A possible methodological explanation may be differences of in vivo and in vitro binding affinities [39]. In this respect, we do not expect a simple linear relationship between mRNA expression and (sst-related) uptake of ^{68}Ga-DOTATOC. For example (Fig. 4b), the direct comparison of normalized sst expression and normalized ^{68}Ga-DOTATOC SUV_{max} shows that in the adrenal gland, kidney and gut sst2 expression exceeds SUV_{max} by up to one order of magnitude. Secondly, using normative data it may be easier to classify a given lesion either as normal, pathologically malignant or pathologically non-malignant on a quantitative basis. Knowledge of normal SUV_{max} data should improve the identification of region-specific advantages or pitfalls. For instance, an intermediate SUV sst2-expressing tumour may have a high tumour to non-tumour contrast when located in bone or lung, appear as cold when located within the spleen or undistinguishable when located within the liver. In this respect, recent data have shown the high sensitivity and specificity of ^{68}Ga-DOTATOC imaging to identify bone metastases of NETs [18]. Another example is the pancreas region, where false sst-positive lesions have been reported, especially in the uncinate process [22]. The presented differences of SUV_{max} between anatomical subdivisions of the pancreas may be the result of differing embryological fates of the ventral and dorsal pancreas reflected in sst expression [4]. Moreover, as for therapy in vivo quantification of individual sst expression within putatively dose-relevant tissues such as the kidneys may help to identify risk factors due to radiopeptide therapy. Then, to account for age- or gender-related influences on normal tissue SUV_{max}, we used a relatively large patient population with a wide age range (no age limitations) and balanced male and female subject numbers. During embryonic development, SOM is expressed in many tissues, but in the adult expression, it mainly occurs in neuroendocrine cells of the brain, intestine and pancreas. Thus, age-related changes of sst expression might be relevant for both development and adult life. Despite the frequent observation of age-dependent decreases of G protein-coupled receptors [40] and the large age range of our study population, our data did not detect any influence of age on the regional SUV_{max}. Concerning this observation it must be considered that earlier ages (<19 years) were not covered by our patients. Thus, our data cannot exclude the necessity of an individual SUV database for younger patients. Moreover, with the exception of thyroid and pancreas, we could exclude significant gender differences of ^{68}Ga-DOTATOC uptake under physiologically normal conditions. Possible implications of gender specificity of sst expression should stimulate further investigations, e.g. in view of different thyroid pathological conditions [10, 14].

Conclusions

In normal human tissues ^{68}Ga-DOTATOC accumulation has been correlated with a basic molecular mechanism, i.e. receptor expression of the sst2 subtype. Taken from routine clinical diagnostics our data have demonstrated ^{68}Ga-DOTATOC uptake SUV_{max} as a robust, age-independent and predominantly gender-independent parameter of normal adult human tissues. A key message from the comparison of phenotype (somatostatin receptor expression) and regional SUV_{max} in normal tissue is that in vivo ^{68}Ga-DOTATOC binding does not correlate with regional sst5 expression. Thus, it may be useless to target multiple sst subtypes by this radiopeptide. Since neuroendocrine tumour manifestations may express significant amounts of non-sst2 somatostatin receptor subtypes, case-adapted sst analogues to optimize tumour targeting have been requested. In this regard, the present normative database may improve the evaluation of novel radiopeptides by means of both the comparison of regional in vivo binding profiles and the relation to regional sst1–sst5 mRNA expression. Evaluating the impact of the normative database under different pathological conditions involving SOM and sst (e.g. imaging of tumour lesions, monitoring of therapeutic response and differential diagnosis of tumour vs inflammation) should be the subject of future clinical research. Finally, diagnosis and therapy using radiopeptides need quantitative data and partial volume effects have to be discussed for both normal tissues and pathological conditions. In this context, the term of a putatively "^{68}Ga-DOTATOC-positive" lesion (e.g. lymphatic node) may be misleading if normal data and partial volume effects are neglected.

Acknowledgements We appreciate the skilful technical support of Julia Joos, Tylay Kilic, Kathrin Klemm, Dipl. Ing. Harald Lahmer, Janina Markese-Asgari, Sandra Schneider, Dr. Jochen Schmitz, Martha Senkowski, Dipl. Ing. Wilfried Sonnenschein, Dipl. Ing. Isabell Stergar, and cand. med. Can Yüksel.

Conflicts of interest None.

References

1. Hoyer D, Bell GI, Berelowitz M, Epelbaum J, Feniuk W, Humphrey PP, et al. Classification and nomenclature of somatostatin receptors. Trends Pharmacol Sci 1995;16:86–8.
2. Lewin MJ. The somatostatin receptor in the GI tract. Annu Rev Physiol 1992;54:455–68.
3. Patel YC. Somatostatin and its receptor family. Front Neuroendocrinol 1999;20:157–98.
4. Ballian N, Brunicardi FC, Wang XP. Somatostatin and its receptors in the development of the endocrine pancreas. Pancreas 2006;33:1–12.
5. Reubi JC, Waser B, Schaer JC, Laissue JA. Somatostatin receptor sst1-sst5 expression in normal and neoplastic human tissues using receptor autoradiography with subtype-selective ligands. Eur J Nucl Med 2001;28:836–46.
6. Burnstock G. Autonomic neurotransmission: 60 years since sir Henry Dale. Annu Rev Pharmacol Toxicol 2009;49:1–30.
7. Van Op den Bosch J, Adriaensen D, Van Nassauw L, Timmermans JP. The role(s) of somatostatin, structurally related peptides and somatostatin receptors in the gastrointestinal tract: a review. Regul Pept 2009;156:1–8.
8. Patel YC, Srikant CB. Somatostatin receptors. Trends Endocrinol Metab 1997;8:398–405.
9. Reubi JC, Schar JC, Waser B, Wenger S, Heppeler A, Schmitt JS, et al. Affinity profiles for human somatostatin receptor subtypes SST1-SST5 of somatostatin radiotracers selected for scintigraphic and radiotherapeutic use. Eur J Nucl Med 2000;27:273–82.
10. Görges R, Kahaly G, Müller-Brand J, Mäcke H, Roser HW, Bockisch A. Radionuclide-labeled somatostatin analogues for diagnostic and therapeutic purposes in nonmedullary thyroid cancer. Thyroid 2001;11:647–59.
11. Gabriel M, Oberauer A, Dobrozemsky G, Decristoforo C, Putzer D, Kendler D, et al. 68Ga-DOTA-Tyr3-octreotide PET for assessing response to somatostatin-receptor-mediated radionuclide therapy. J Nucl Med 2009;50:1427–34.
12. Rominger A, Saam T, Vogl E, Ubleis C, la Fougère C, Förster S, et al. In vivo imaging of macrophage activity in the coronary arteries using 68Ga-DOTATATE PET/CT: correlation with coronary calcium burden and risk factors. J Nucl Med 2010;51:193–7.
13. van Hagen PM, Dalm VA, Staal F, Hofland LJ. The role of cortistatin in the human immune system. Mol Cell Endocrinol 2008;286:141–7.
14. Lincke T, Singer J, Kluge R, Sabri O, Paschke R. Relative quantification of indium-111 pentetreotide and gallium-68 DOTA-TOC uptake in the thyroid gland and association with thyroid pathologies. Thyroid 2009;19:381–9.
15. Dalm VA, van Hagen PM, van Koetsveld PM, Achilefu S, Houtsmuller AB, Pols DH, et al. Expression of somatostatin, cortistatin, and somatostatin receptors in human monocytes, macrophages, and dendritic cells. Am J Physiol Endocrinol Metab 2003;285:E344–53.
16. Hofmann M, Maecke H, Börner R, Weckesser E, Schöffski P, Oei L, et al. Biokinetics and imaging with the somatostatin receptor PET radioligand (68)Ga-DOTATOC: preliminary data. Eur J Nucl Med 2001;28:1751–7.
17. Ruf J, Heuck F, Schiefer J, Denecke T, Elgeti F, Pascher A, et al. Impact of multiphase 68Ga-DOTATOC-PET/CT on therapy management in patients with neuroendocrine tumors. Neuroendocrinology 2010;91:101–9.
18. Putzer D, Gabriel M, Henninger B, Kendler D, Uprimny C, Dobrozemsky G, et al. Bone metastases in patients with neuroendocrine tumor: 68Ga-DOTA-Tyr3-octreotide PET in comparison to CT and bone scintigraphy. J Nucl Med 2009;50:1214–21.
19. Corleto VD, Falconi M, Panzuto F, Milione M, De Luca O, Perri P, et al. Somatostatin receptor subtypes 2 and 5 are associated with better survival in well-differentiated endocrine carcinomas. Neuroendocrinology 2009;89:223–30.
20. Barone R, Borson-Chazot F, Valkema R, Walrand S, Chauvin F, Gogou L, et al. Patient-specific dosimetry in predicting renal toxicity with (90)Y-DOTATOC: relevance of kidney volume and dose rate in finding a dose-effect relationship. J Nucl Med 2005;46 Suppl 1:99S–106S.
21. Cremonesi M, Botta F, Di Dia A, Ferrari M, Bodei L, De Cicco C, et al. Dosimetry for treatment with radiolabelled somatostatin analogues. A review. Q J Nucl Med Mol Imaging 2010;54:37–51.
22. Prasad V, Baum RP. Biodistribution of the Ga-68 labeled somatostatin analogue DOTA-NOC in patients with neuroendocrine tumors: characterization of uptake in normal organs and tumor lesions. Q J Nucl Med Mol Imaging 2010;54:61–7.

23. Zhernosekov KP, Filosofov DV, Baum RP, Aschoff P, Bihl H, Razbash AA, et al. Processing of generator-produced 68Ga for medical application. J Nucl Med 2007;48:1741–8.
24. Jentzen W. Experimental investigation of factors affecting the absolute recovery coefficients in iodine-124 PET lesion imaging. Phys Med Biol 2010;55:2365–98.
25. Ziegler CG, Brown JW, Schally AV, Erler A, Gebauer L, Treszl A, et al. Expression of neuropeptide hormone receptors in human adrenal tumors and cell lines: antiproliferative effects of peptide analogues. Proc Natl Acad Sci U S A 2009;106:15879–84.
26. Ueberberg B, Tourne H, Redmann A, Walz MK, Schmid KW, Mann K, et al. Differential expression of the human somatostatin receptor subtypes sst1 to sst5 in various adrenal tumors and normal adrenal gland. Horm Metab Res 2005;37:722–8.
27. Ueberberg B, Unger N, Sheu SY, Walz MK, Schmid KW, Saeger W, et al. Differential expression of ghrelin and its receptor (GHS-R1a) in various adrenal tumors and normal adrenal gland. Horm Metab Res 2008;40:181–8.
28. Campana D, Ambrosini V, Pezzilli R, Fanti S, Labate AM, Santini D, et al. Standardized uptake values of (68)Ga-DOTANOC PET: a promising prognostic tool in neuroendocrine tumors. J Nucl Med 2010;51:353–9.
29. Koukouraki S, Strauss LG, Georgoulias V, Eisenhut M, Haberkorn U, Dimitrakopoulou-Strauss A. Comparison of the pharmacokinetics of 68Ga-DOTATOC and [18F]FDG in patients with metastatic neuroendocrine tumours scheduled for 90Y-DOTATOC therapy. Eur J Nucl Med Mol Imaging 2006;33:1115–22.
30. Froidevaux S, Eberle AN, Christe M, Sumanovski L, Heppeler A, Schmitt JS, et al. Neuroendocrine tumor targeting: study of novel gallium-labeled somatostatin radiopeptides in a rat pancreatic tumor model. Int J Cancer 2002;98:930–7.
31. Kessler RM, Ellis Jr JR, Eden M. Analysis of emission tomographic scan data: limitations imposed by resolution and background. J Comput Assist Tomogr 1984;8:514–22.
32. Reubi JC, Waser B, Schaer JC, Laissue JA. Somatostatin receptor sst1-sst5 expression in normal and neoplastic human tissues using receptor autoradiography with subtype-selective ligands. Eur J Nucl Med 2001;28:836–46.
33. Zilles K, Palomero-Gallagher N, Grefkes C, Scheperjans F, Boy C, Amunts K, et al. Architectonics of the human cerebral cortex and transmitter receptor fingerprints: reconciling functional neuroanatomy and neurochemistry. Eur Neuropsychopharmacol 2002;12:587–99.
34. Ludvigsen E, Olsson R, Stridsberg M, Janson ET, Sandler S. Expression and distribution of somatostatin receptor subtypes in the pancreatic islets of mice and rats. J Histochem Cytochem 2004;52:391–400.
35. Bhandari S, Watson N, Long E, Sharpe S, Zhong W, Xu SZ, et al. Expression of somatostatin and somatostatin receptor subtypes 1–5 in human normal and diseased kidney. J Histochem Cytochem 2008;56:733–43.
36. Low MJ. Clinical endocrinology and metabolism. The somatostatin neuroendocrine system: physiology and clinical relevance in gastrointestinal and pancreatic disorders. Best Pract Res Clin Endocrinol Metab 2004;18:607–22.
37. Bryant MG, Bloom SR, Polak JM, Hobbs S, Domschke W, Domschke S, et al. Measurement of gut hormonal peptides in biopsies from human stomach and proximal small intestine. Gut 1983;24:114–9.
38. Smith WH, Nair RU, Adamson D, Kearney MT, Ball SG, Balmforth AJ. Somatostatin receptor subtype expression in the human heart: differential expression by myocytes and fibroblasts. J Endocrinol 2005;187:379–86.
39. Eckelman WC. The application of receptor theory to receptor-binding and enzyme-binding oncologic radiopharmaceuticals. Nucl Med Biol 1994;21:759–69.
40. Meyer PT, Elmenhorst D, Boy C, Winz O, Matusch A, Zilles K, et al. Effect of aging on cerebral A1 adenosine receptors: a [18F]CPFPX PET study in humans. Neurobiol Aging 2007;28:1914–24.